Decay of Shock Waves in Detonation-Driven Shock Tubes, Donner T. Schoeffler and Joseph E. Shepherd, California Institute of Technology, Pasadena, CA, USA. Presented at the 34th International Symposium on Shock Waves (ISSW34), Daegu, Korea , 16-21 July 2023.

Decay of Shock Waves in Detonation-Driven Shock Tubes

D. T. Schoeffler and J. E. Shepherd
California Institute of Technology, Pasadena, CA, 91125, United States

Corresponding author's email address: dschoeff@caltech.edu

Abstract

Shock waves generated in forward-mode detonation-driven shock tubes are intrinsically unsteady. Application of detonation drivers in research facilities is fundamentally limited by the extent to which the test flow is made unsteady by the decaying shock wave. Numerical simulations of a simple model problem are used to study the effect of independent variables on the shock decay. The time evolution of all decaying shock waves is shown to be excellently modeled by a single power law, which is used to quantify shock decay properties across all cases. Results indicate that shock unsteadiness is strongly correlated with shock tube sound speed ratio, and its reduction may mitigate the influence of shock unsteadiness on test flows.

1 Introduction

Detonation waves generate high pressures, temperatures, and gas velocities that may be used to drive strong shock waves in shock tubes. The high performance of detonation drivers from relatively modest initial pressures makes them attractive for use in hypervelocity flow facilities, such as shock tunnels and expansion tubes. However, an essential characteristic of detonation drivers is that the nonuniform driver gas causes the driven shock wave to decay from the beginning of its formation. Prediction of the shock decay is essential not only to properly choose the shock's strength for processing the test gas, but also because the decaying shock introduces unsteadiness in the post-shock flow, which can pose serious limitations for facilities where the test gas is meant to simulate some steady, hypervelocity flow. Nonetheless, unsteady shock waves may be used if the time scale of their unsteadiness is sufficiently large compared to a facility's test time. Despite many studies on detonation drivers [1–4], including their implementation in several large research facilities [5–7], there is no model for the driven shock decay. Without further development, methods of geometrical shock dynamics [8] including higher-order generalizations [9] are not appropriate for this problem where all shock decay results from post-shock gradients. Self-similar blast wave solutions [10] use a point explosion assumption that is inapplicable here, where shock propagation occurs over lengths comparable to the detonation driver length.

Without analytical methods, numerical simulations of a model problem provide essential insight and lead to both useful results describing detonation-driven shocks and potential directions for theoretical development. To this end, a model problem is first formulated, where the key independent variables are identified and a technique for characterizing the shock decay is proposed in the form of a propagation law. Methods used for numerical simulation and post-processing are described. Results provide a complete picture of the shock's evolution over time. The propagation law is shown to be an exceptional model for the decaying shock, and it is used to quantify how properties of the decay are influenced by independent variables. Effects of the shock tube pressure ratio and sound speed ratio are principally examined, and insensitivity to the remaining variables is verified. Correlations

are given so that for a wide range of relevant shock tube conditions, the shock Mach number and decay rate can be computed to provide estimates important for analysis of any detonation-driven shock tube research facility.

2 Problem formulation

The focus of this study is on forward-mode detonation drivers, where the detonation propagates downstream and directly impacts the shock tube diaphragm. Only the one-dimensional driven shock propagation is of interest. Reverse-mode operation requires detonation initiation at the shock tube diaphragm, which includes facility-specific transients that are not as amenable to the one-dimensional approximations used here.

The intrinsically multidimensional cellular detonation structure can be modeled as a one-dimensional reaction zone in a spanwise mean, terminating in the equilibrium Chapman-Jouguet (CJ) state. Behind the CJ state is an unsteady expansion wave, known as the Taylor-Zel'dovich (TZ) wave when self-similar. Two length scales are present in this formulation of the one-dimensional detonation wave: the reaction zone width and the detonation propagation distance, i.e., the driver length. The reaction zone width scales with some characteristic detonation cell size, which is typically small compared to the driver length for all pressures and mixtures of interest here. So, the reaction zone may be neglected from analysis, and the CJ-TZ detonation structure remains. Additionally, wall effects like heat transfer are neglected, which is appropriate for sufficiently small driver length-to-diameter ratios.

Both the inert shock tube gas and detonation products are assumed to be perfect gases and chemically frozen. Although the CJ state can be adequately approximated this way, additional equilibration of hot detonation products in the TZ wave is known to occur [11] and can also be expected in the reflected rarefaction wave. For the large shock Mach numbers of interest here, heat capacities are also expected to be nonconstant. These real gas effects are important, although their impact on the results presented here remains to be quantified. Results for perfect gases provide the essential insight into the fundamental gas dynamics from which generalization to other considerations may be made.

The initial condition for the detonation-driven shock tube, as modeled here, is when the CJ state is incident with the contact surface separating shock tube sections. The typical enumeration of shock tube gas states is used here with a modification to also describe relevant states in the detonation driver, which are the initial, unreacted gas state 41, the CJ state 42, and the TZ wave plateau state 43. These subscripts are used throughout, particularly for the CJ state. Because of the self-similar TZ wave, all length scales can be normalized by the driver length. The resulting simplified model problem has six independent, nondimensional variables describing all cases. They are

$$\frac{P_{42}}{P_1}, \quad \frac{a_{42}}{a_1}, \quad M_{42}, \quad \gamma_{42}, \quad \gamma_1, \quad \frac{W_{42}}{W_1}\,, \tag{1}$$

which are, respectively, the pressure ratio, the sound speed ratio, the local CJ Mach number in the lab-frame, the CJ gas specific heat ratio, the shock tube gas specific heat ratio, and the ratio of molecular weights. The only additional variable not present in typical shock tube analysis is $M_{42} = u_{42}/a_{42}$, which quantifies the driver gas velocity in the lab-frame. The molecular weight ratio is only included as it is necessary to compute the temperature, which is unimportant for the present problem. The nonuniformity from the TZ wave is a result of the boundary conditions and does not require any additional variables to describe.

All quantities in (1) were independently investigated here. A base parameter set is used throughout the study to vary parameters about. Quantities for the base case are

$$\frac{P_{42}}{P_1} = 200, \quad \frac{a_{42}}{a_1} = 3.7, \quad M_{42} = 0.85, \quad \gamma_{42} = 1.14, \quad \gamma_1 = 1.4, \quad \frac{W_{42}}{W_1} = 0.79\ , \tag{2}$$

which were chosen to be values typical for stoichiometric ethylene-oxygen at standard temperature and pressure and air driven gas, although they are typical for other mixtures as well. The initial condition given by the base case is shown in Figure 1. The primary variables considered for shock tube operation were the pressure ratio and sound speed ratio. Quantities M_{42} and γ_{42} are only determined by the detonation gas mixture, and typical values for many mixtures are $M_{42} \in [0.8, 0.85]$ and $\gamma_{42} \in [1.1, 1.2]$. The only parameter for the inert shock tube gas is γ_1.

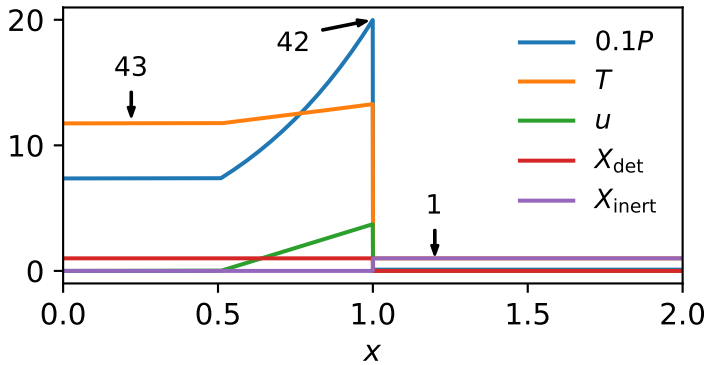

Figure 1: Initial conditions for the simplified model in terms of pressure, temperature, velocity, and mole fractions for detonation driver gas, X_{det}, and inert shock tube gas, X_{inert}, where enumeration 42 and 43 identifies the CJ and TZ-plateau states, respectively

Although the evolution of the initial condition is numerically simulated, the initial speed of the driven shock can be directly computed using a pressure-velocity diagram. Because of the nonzero gas velocity, either a rarefaction or shock may be reflected from the contact surface interaction, determined by the position of the CJ state relative to the shock curve. All simulation cases were chosen to be on the side of the boundary where an expansion is reflected. Cases used to examine the effect of only pressure and sound speed ratios are plotted with the wave-reflection boundary in Figure 2. Shock tube conditions in which a shock is reflected are discussed elsewhere [3]. For the cases where a rarefaction wave is reflected, the initial shock Mach number, M_0, is given by a modification to the typical shock tube equation,

$$\frac{P_{42}}{P_1} = \frac{1 + \dfrac{2\gamma_1}{\gamma_1 + 1}(M_0^2 - 1)}{\left(1 - \dfrac{\gamma_{42} - 1}{\gamma_1 + 1}\dfrac{a_1}{a_{42}}\dfrac{M_0^2 - 1}{M_0} + \dfrac{\gamma_{42} - 1}{2}M_{42}\right)^{\frac{2\gamma_{42}}{\gamma_{42}-1}}}\ . \tag{3}$$

In order to characterize the decaying shock wave generally, it is useful to define a decay parameter, δ, where the time-varying shock Mach number, $M(t)$, is normalized by its initial speed, M_0, i.e.,

$$\delta = \frac{M(t)}{M_0}\ . \tag{4}$$

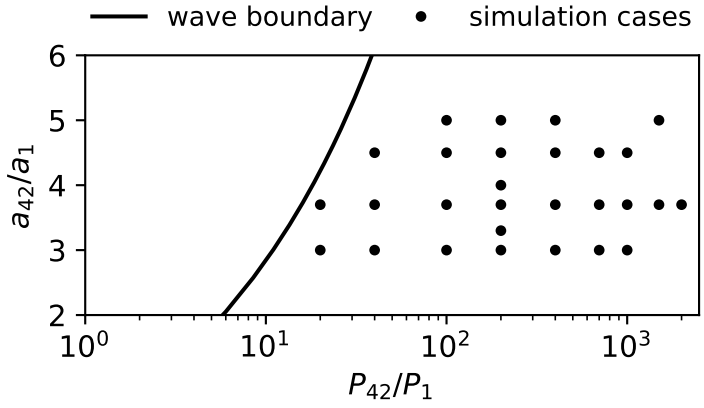

Figure 2: Map of variables for simulation cases examining the combined effects of pressure and sound speed ratios. All are located to the right of the boundary defining reflection of expansion or shock waves at the diaphragm for $M_{42} = 0.85$, $\gamma_{42} = 1.14$, and $\gamma_1 = 1.4$

The formulation in (4) is only one candidate and might be considered appropriate for a strong shock.

In order to provide a general description for the propagation of all decaying shock waves in the present numerical simulations, the following shock propagation law is proposed,

$$\delta = \frac{1}{(1 + \beta t/\alpha)^{\alpha}} \,, \tag{5}$$

where β is the positive initial decay rate, $\beta = -\dot{\delta}_0$, and normalizes the time variable. The power, α, characterizes the shape of the trajectory. Larger values of α correspond with faster decay for a given value of β. Both parameters determine the rate of shock decay and hence the magnitude of unsteadiness generated in the post-shock flow. This formulation of the shock decay will be justified below from simulation results and discussed further.

3 Simulation methods

Evolution of the detonation-driven shock tube initial condition was directly simulated using the open-source finite-volume CFD toolbox OpenFOAM-7 [12]. The particular solver used was adapted from an additional library blastFoam-4 [13], where conservation equations for mass, momentum, energy, and species are solved for inviscid, non-heat-conducting, perfect gases. Solution methods are typical to other OpenFOAM solvers [14], where fluxes are interpolated using the scheme by Kurganov et al. [15] and limited using the functions by van Albada [16] for density and van Leer [17] for all other variables. Second-order Runge-Kutta time integration was used, as implemented in blastFoam.

Simulations were performed using variables normalized by the inert shock tube gas initial state, i.e.,

$$P = \frac{\tilde{P}}{\tilde{P}_1}, \quad T = \frac{\tilde{T}}{\tilde{T}_1}, \quad u = \frac{\tilde{u}}{\tilde{u}_{\text{ref}}}, \quad W = \frac{\tilde{W}}{\tilde{W}_1}, \quad t = \frac{\tilde{t}\tilde{u}_{\text{ref}}}{\tilde{L}}, \quad x = \frac{\tilde{x}}{\tilde{L}} \,, \tag{6}$$

where $\tilde{u}_{\text{ref}} = \sqrt{\tilde{R}\tilde{T}_1/W_1}$, $\tilde{R}$ is the universal gas constant, $\tilde{L}$ is the driver length, and the tilde identifies dimensional quantities. Simulation results are reported below using the

same normalizations except for the reference velocity, where the sound speed, a_1, is used instead. The sound speed and $\tilde{u}_{\text{ref}}$ are related by $\tilde{a}_1/\tilde{u}_{\text{ref}} = \sqrt{\gamma_1}$, hence simulation time is reported with a square-root gamma factor.

For a given set of shock tube variables, the initial condition was computed separately, discretely sampled, and mapped onto a uniform simulation grid, from which the simulation was initiated. All simulation cases were run until the major features of the shock evolution were developed, typically $t_{\text{sim}} \geq 3.0\sqrt{\gamma_1}$. Time steps were sampled every $\Delta t = 0.001\sqrt{\gamma_1}$.

The driven shock Mach number was computed in post-processing at each sampled time step using the post-shock pressure and the perfect gas shock jump equation. Numerically differentiating discrete simulation data is prone to introducing large errors and then necessitates substantial use of smoothing algorithms. Using the post-shock pressure for the shock Mach number is a repeatable technique that minimizes use of smoothing methods and reduces the error introduced into computed quantities. The time evolution of the shock velocity exhibits several kinks, which were identified using the large spikes in the second derivative of shock velocity after smoothing the data with a Savitzky-Golay filter. No smoothing is otherwise applied to the shock Mach number results presented below.

Numerical simulations and post-processing algorithms were both verified for grid independence using the base case with grid resolutions of $1 \cdot 10^3$, $2 \cdot 10^3$, and $4 \cdot 10^3$ cells per driver length. All simulations presented here used $2 \cdot 10^3$ cells per driver length, and the shock tube length was varied depending on the case so that all shocks reached similar points in their evolution. Total cell count for each case ranged from $4 \cdot 10^4$ to $8 \cdot 10^4$.

Results from thirty seven simulations are described below, which examined the influence of all independent variables. Primary focus was on the effect of pressure and sound speed ratios, and the twenty eight pertaining simulation variables are shown in Figure 2. Sensitivity of the base case to other variables was examined with cases where $\gamma_{42} \in \{1.1, 1.14, 1.2\}$, $M_{42} \in \{0.8, 0.825, 0.85\}$, and $\gamma_1 \in \{1.2, 1.3, 1.4, 1.5, 1.66\}$.

4 Results and discussion

The time evolution of the driven shock Mach number for the base set of independent variables (2) is shown in Figure 3. The Mach number continuously decays from the initial speed to an apparently quasi-steady plateau period, after which the shock continues to decay further. These three periods of the shock Mach number evolution were obtained in all simulations.

A space-time diagram of the base simulation case was computed by directly integrating along the characteristics. The result is shown in Figure 4, where the reflection of characteristics at the end wall and shock front are tracked. Characteristic reflections at the contact surface are important but not included here. The space-time diagram illustrates the origin of the three regions of the shock Mach number evolution shown in Figure 3. The shock initially decays from attenuation by the transmitted TZ wave. However, since the TZ wave is finite, once the final characteristic intersects the shock, a region of approximately steady propagation is reached. After sufficient time, the centered expansion wave from the initial contact surface interaction reflects from the driver end wall and catches up with the shock wave, which causes it to decay further.

The plateau period is referred to as quasi-steady because the shock Mach number is not exactly constant. The variation that does occur is substantially smaller than the variation during periods of shock decay, such that the plateau period is comparably steady. Unsteadiness in this period results from wave interaction with the contact surface, however

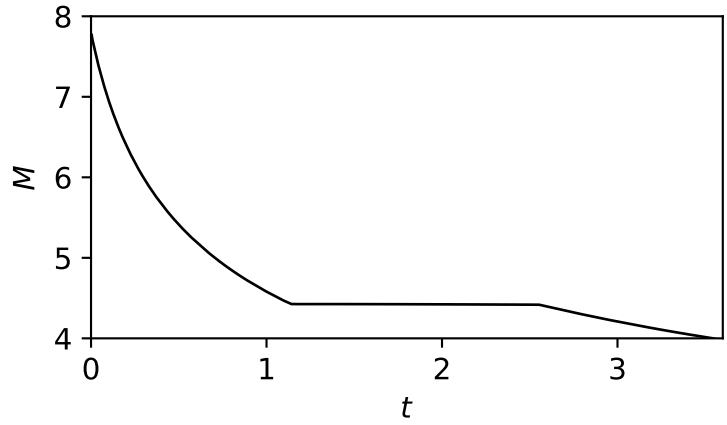

Figure 3: Time evolution of driven shock Mach number for simulation of base case

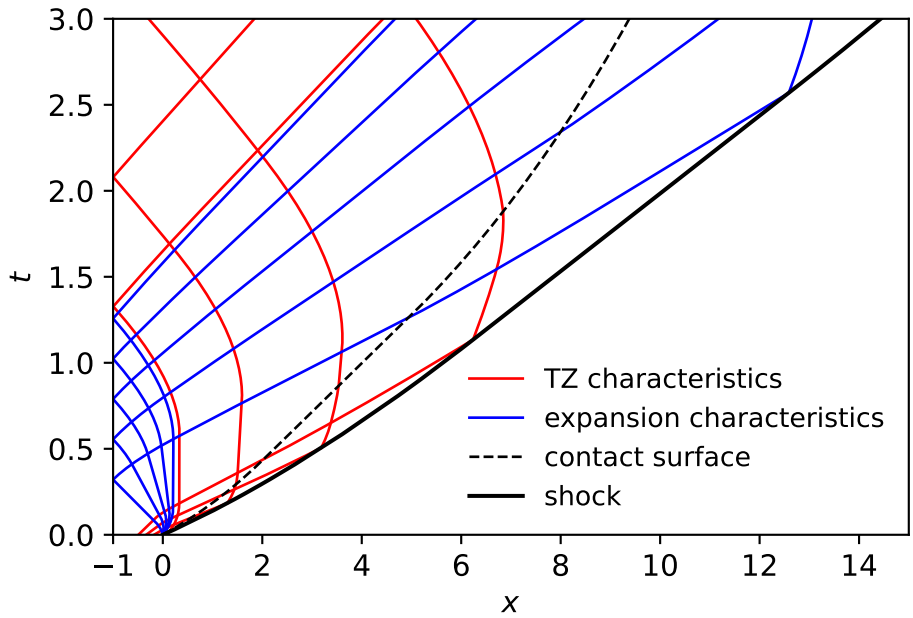

Figure 4: Space-time diagram generated from integration along characteristics of simulation data for the base parameter set

analysis of these phenomena is the subject of future work. For now it is noted that the shock Mach number in this period can be well approximated by the shock tube equation (7) expressed in terms of the TZ plateau properties, i.e., P_{43}/P_1 and a_{43}/a_1. This makes the additional assumption that the post-shock gas is homentropic, which is false, although Figure 5 shows that the model provides a good prediction for the mean shock Mach number in the plateau period for all simulation cases.

$$\frac{P_{43}}{P_1} = \frac{1 + \dfrac{2\gamma_1}{\gamma_1 + 1}(M_\mathrm{p}^2 - 1)}{\left(1 - \dfrac{\gamma_{42} - 1}{\gamma_1 + 1}\dfrac{a_1}{a_{43}}\dfrac{M_\mathrm{p}^2 - 1}{M_\mathrm{p}}\right)^{\frac{2\gamma_{42}}{\gamma_{42}-1}}} \tag{7}$$

Even for moderate pressure ratios, the quasi-steady plateau period is only reached

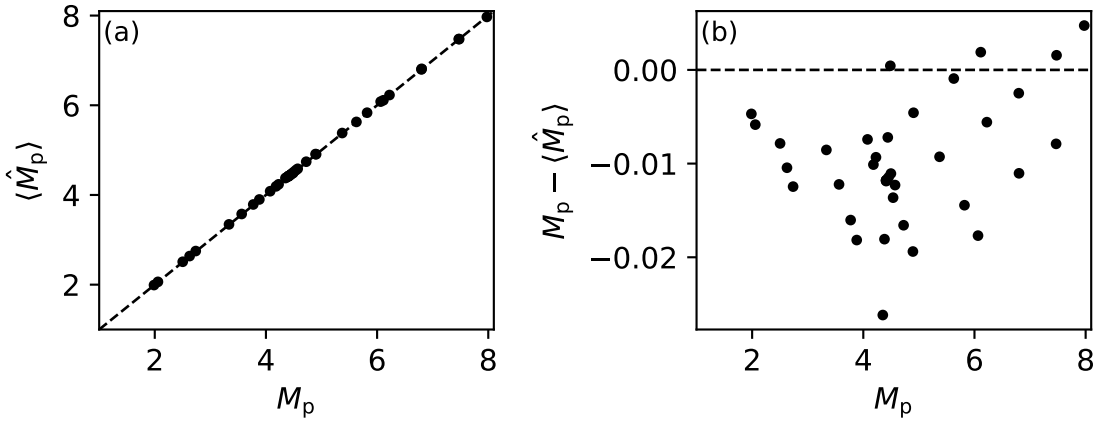

Figure 5: (a) Comparison of the mean shock Mach number in the plateau region from numerical simulations, $\langle \hat{M}_\mathrm{p} \rangle$, with the result from the model, M_p, given by (7). Residuals are shown in (b)

after the shock has traveled several driver lengths. Reverse-mode detonation drivers utilize this condition by initiating the detonation at the diaphragm and reducing the effective TZ wave or driver length. It is unrealistic to access this plateau period in foward-mode operation without using shock initiation to shorten the TZ wave [5]. Therefore, in order to otherwise use the forward-mode driver, the driven shock wave during its initial period of decay must be exploited, which requires a characterization of its decay properties.

The shock decay parameter (4) in the first period of shock decay was fit to the propagation law (5) for all simulation cases, and both the fit and its residuals are shown in Figure 6. The root-mean-square error between data and fit across all simulations is $7 \cdot 10^{-4}$, proving the propagation law to describe the shock decay exceptionally well. The conclusions from this are several-fold. Foremost, the decaying shock propagates according to a power law in time as formulated by (5) to within some negligible error. There are only two properties of this propagation: the decay power, α, and the time scale or initial decay rate, β. The fitting of simulation data to (5) therefore provides measurements of these quantities, α and β, which may be used to examine effects of independent variables on the resulting shock decay.

The shock decay properties, α and β, for simulations where the pressure and sound speed ratios were varied together are plotted against correlations in Figure 7. The decay power, α, could be separated into a linear combination of independent functions of the pressure and sound speed ratios. Dependence on the sound speed ratio could be linearly fit, but a more complicated dependence on the pressure ratio required a cubic fit to the logarithm. Although cumbersome and not theoretically motivated, the functional form was chosen because it effectively fits the data. The pressure ratio dependence exhibits a maximum at $P_{42}/P_1 \approx 160$. Increasing the pressure ratio further decreases α. Decreasing the sound speed ratio decreases α. The correlation for β in (b) shows that the initial decay rate increases strongly with increasing the sound speed ratio and decreases with increasing the pressure ratio. This is important for facility operation. In order to reduce unsteadiness in the test gas it is desired to reduce the decay rate of the shock wave. This can be done by increasing the pressure ratio and decreasing the sound speed ratio, which has the double effect of reducing the decay power, α, and decreasing the initial decay rate, β. Dependence of β on the sound speed ratio is particularly strong, nearly quadratic. For

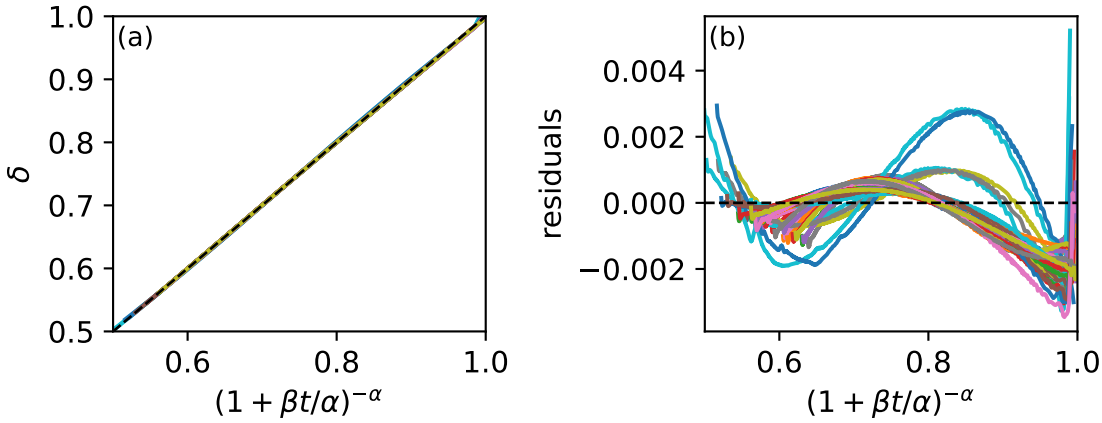

Figure 6: (a) The shock decay parameter (4) for all simulation cases is plotted against a fit to the propagation law (5) with corresponding residuals plotted in (b), where residuals are $\delta - (1+\beta t/\alpha)^{-\alpha}$

example, a reduction of sound speed ratio from 3.7 to 3 reduces the initial decay rate by 30%. Since the shock Mach number is directly proportional to both the pressure and sound speed ratios, the ratios can be varied to preserve the same shock Mach number while decreasing the shock unsteadiness.

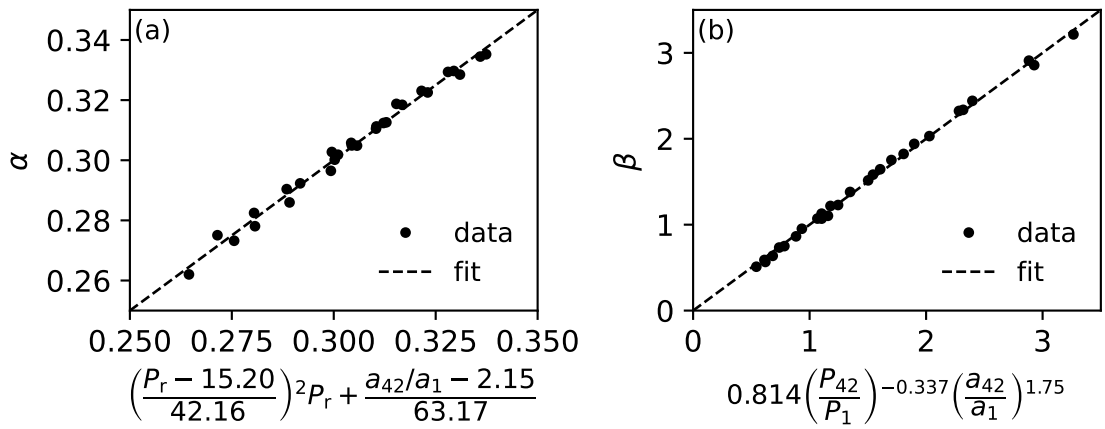

Figure 7: Shock decay properties plotted against multivariable correlations with pressure and sound speed ratios, where $P_r = \log(P_{42}/P_1)$

The other three independent variables of interest are γ_1, γ_{42}, and M_{42}. Figure 8 plots α and β for simulation cases where the base case is perturbed about these three variables independently. For all, the variation in both α and β is small, less than 3% for the variable ranges tested, which confirms that the effects of pressure and sound speed ratios are primary. A single simulation case with unity molecular weight ratio was performed to confirm its irrelevance to the present problem. Results were identical to the base case, except in the temperature variable, as expected.

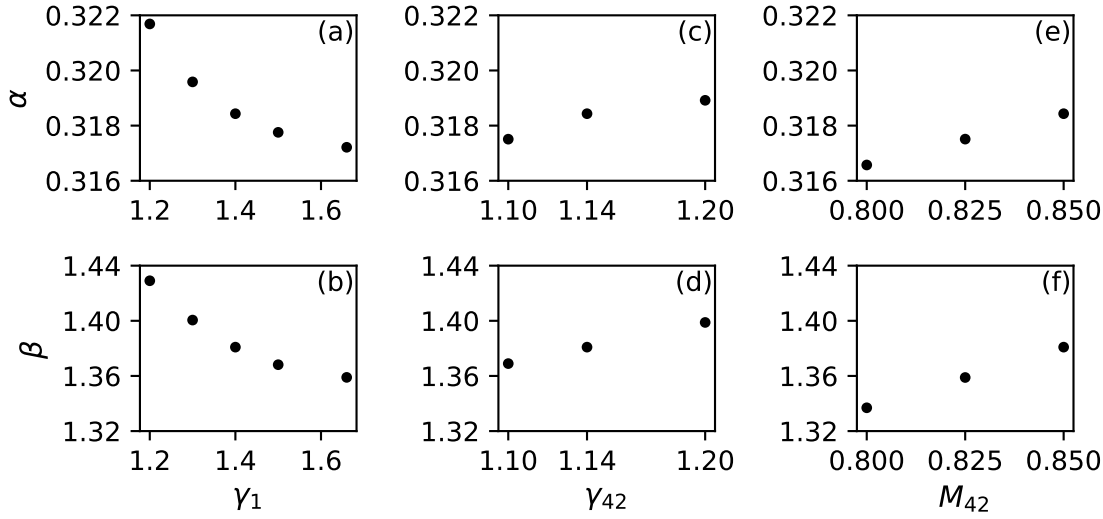

Figure 8: Decay properties from sensitivity study of secondary independent variables, where each quantity was varied individually about the base case

5 Conclusion

Exceptional agreement between the functional form of a shock propagation law and simulation data for decaying shock waves enabled fits to the propagation law to be used as measurements of shock decay properties, namely a decay power, α, and initial decay rate, β. The decay properties for detonation-driven shock waves were found to be principally dependent on shock tube pressure and sound speed ratios. A strong dependence on the sound speed ratio indicates that it is desirable to operate forward-mode detonation drivers with hydrocarbon fuels and potentially diluted with heavy gases to decrease the sound speed. Conversely, it may be desirable to increase the shock decay rate in reverse-mode or shock-initiated forward-mode operation, so that initial transients are attenuated rapidly to acquire the desired steady shock.

A simple model problem was used for this analysis. However, the success of the propagation law suggests it might be useful for characterizing decaying shock waves more generally, for example, in experiments where decaying shock waves are influenced by facility-specific nonidealities, finite detonation thicknesses, and real gas effects.

6 Acknowledgments

This work was sponsored by the Office of Naval Research (ONR), under grant number N00014-22-1-2141. The views and conclusions contained herein are those of the authors only and should not be interpreted as representing those of ONR, the U.S. Navy or the U.S. Government.

References

[1] Coates, P. B. and Gaydon, A. G. A Simple Shock Tube with Detonating Driver Gas. *Proc. Math. Phys. Sci.*, 283(1392):18–32, 1965. doi: 10.1098/rspa.1965.0004.

[2] Yu, H. r., Esser, B., Lenartz, M., and Grönig, H. Gaseous detonation driver for a shock tunnel. *Shock Waves*, 2(4):245–254, December 1992. doi: 10.1007/BF01414760.

[3] Peace, J. T. and Lu, F. K. Detonation-to-shock wave transmission at a contact discontinuity. *Shock Waves*, 28(5):981–992, 2018. doi: 10.1007/s00193-018-0804-6.

[4] Jayamani, A. and Lu, F. K. Method-of-characteristics model for a low-enthalpy, detonation-driven shock tube. *Physics of Fluids*, 34(6):066109, June 2022. doi: 10.1063/5.0093888.

[5] Bakos, R., Calleja, J., Erdos, J., Sussman, M., and Wilson, G. An experimental and computational study leading to new test capabilities for the HYPULSE facility with a detonation driver. In *Advanced Measurement and Ground Testing Conference*, New Orleans, LA, U.S.A., June 1996. American Institute of Aeronautics and Astronautics. doi: 10.2514/6.1996-2193.

[6] Jiang, Z. and Yu, H. Development and Calibration of Detonation-Driven High-Enthalpy and Hypersonic Test Facilities. In *Experimental Methods of Shock Wave Research*, pages 285–313. Springer International Publishing, 2016. doi: 10.1007/978-3-319-23745-9_9.

[7] Olivier, H. The Aachen Shock Tunnel TH2 with Dual Driver Mode Operation. In Igra, O. and Seiler, F., editors, *Experimental Methods of Shock Wave Research*, pages 111–129. Springer International Publishing, Cham, 2016. doi: 10.1007/978-3-319-23745-9_5.

[8] Whitham, G. B. *Linear and Nonlinear Waves*. John Wiley & Sons, Ltd, 1999.

[9] Best, J. P. A generalisation of the theory of geometrical shock dynamics. *Shock Waves*, 1(4):251–273, December 1991. doi: 10.1007/BF01418882.

[10] Sedov, L. I. *Similarity and Dimensional Methods in Mechanics*. Academic Press, 1959. doi: 10.1016/C2013-0-08173-X.

[11] Cooper, M. A. *Impulse Generation by Detonation Tubes*. phd, California Institute of Technology, 2004. URL `https://resolver.caltech.edu/CaltechETD:etd-05252004-164627`.

[12] OpenFOAM. URL `https://openfoam.org/`.

[13] blastFoam: A solver for compressible multi-fluid flow with application to high-explosive detonation, April 2020. URL `https://github.com/synthetik-technologies/blastfoam`.

[14] Greenshields, C. J., Weller, H. G., Gasparini, L., and Reese, J. M. Implementation of semi-discrete, non-staggered central schemes in a colocated, polyhedral, finite volume framework, for high-speed viscous flows. *Int. J. Numer. Meth. Fluids*, 2009. doi: 10.1002/fld.2069.

[15] Kurganov, A., Noelle, S., and Petrova, G. Semidiscrete Central-Upwind Schemes for Hyperbolic Conservation Laws and Hamilton–Jacobi Equations. *SIAM J. Sci. Comput.*, 23(3):707–740, January 2001. doi: 10.1137/S1064827500373413.

[16] van Albada, G. D., van Leer, B., and Roberts, W. W. A Comparative Study of Computational Methods in Cosmic Gas Dynamics. In Hussaini, M. Y., van Leer, B., and Van Rosendale, J., editors, *Upwind and High-Resolution Schemes*, pages 95–103. Springer, Berlin, Heidelberg, 1997. doi: 10.1007/978-3-642-60543-7_6.

[17] van Leer, B. Towards the ultimate conservative difference scheme. II. Monotonicity and conservation combined in a second-order scheme. *Journal of Computational Physics*, 14(4):361–370, March 1974. doi: 10.1016/0021-9991(74)90019-9.